View metadata, citation and similar papers at core.ac.uk
brought to you by CORE
provided by CiteSeerX

128 *Journal of Electrical Engineering & Technology Vol. 6, No. 1, pp. 128~132, 2011*
DOI: 10.5370/JEET.2011.6.1. 128

Generation of Non-uniform Meshes for Finite-Difference Time-Domain Simulations

Hyeong-Seok Kim†, Insung Ihm* and Kyung Choi**

Abstract - In this paper, two automatic mesh generation algorithms are presented. The methods seek to optimize mesh density with regard to geometries exhibiting both fine and coarse physical structures. When generating meshes, the algorithms attempt to satisfy the conditions on the maximum mesh spacing and the maximum grading ratio simultaneously. Both algorithms successfully produce non-uniform meshes that satisfy the requirements for finite-difference time-domain simulations of microwave components. Additionally, an algorithm successfully generates a minimum number of grid points while maintaining the simulation accuracy.

Keywords: Mesh generation, Finite-difference, Time-domain, Microprocessor applications

1. Introduction

For effective analysis of electromagnetic waves using finite-difference time-domain (FDTD) simulations [1]-[4], it is important to produce a high quality of mesh for a given geometry to achieve better accuracy and frequency resolution. Simple uniform rectangular meshes are frequently used in the tessellation. However, they often entail an enormous number of cells when structures with fine details have to be resolved precisely. A more efficient method is to generate non-uniform meshes that adapt grid spacing according to the geometric properties of the structures while maintaining the grading ratio between adjacent cells. This paper presents automatic 3D mesh generation techniques that produce effective non-uniform rectangular meshes. Our techniques attempt to minimize the number of mesh cells, while satisfying user-imposed requirements on maximum mesh spacing and maximum grading ratio. To evaluate the effectiveness of proposed algorithms, a complex structured 3D RF model is chosen and the analysis results are compared with other commercial ones.

2. Problem Definition

A 3D domain may include geometries composed of elementary objects, such as axis-aligned rectangular parallelepipeds (cuboids), spheres, or axis-aligned cylinders. Each elementary object is associated with a respective upper limit, $d_{\max}$, on the maximum grid spacing, which require that cells inside the object may not have edges longer than the imposed limit.

Fig. 1 illustrates a projection on the x-axis. It consists of m = 10 intervals where each interval is associated with length d_i and upper limit $d_i^{\max}$, inherited from the projected objects. Tessellation of 3D models is achieved using adaptive subdivision of the three sets of 1D intervals. To generate an effective non-uniform rectangular mesh, we impose the following three requirements on the 1D interval tessellation problem:

1. Minimization requirement - Minimize the number of subintervals generated as a result of tessellating the initial subdivision intervals. This condition is necessary to optimize the time and space complexity of the analysis process.
2. $d_i^{\max}$ requirement - The lengths of all tessellated subintervals in the ith interval must be shorter than $d_i^{\max}$. This condition is necessary to satisfy the analysis precision, which is constrained by the mesh spacing.

Even more, $d_i^{\max}$ do not exceed either the limit of stability criterion of a numerical analysis for the 1st order analysis of FDTD in previous work [5] and the 2nd order analysis [6]. This constraint can be additionally imposed by user.

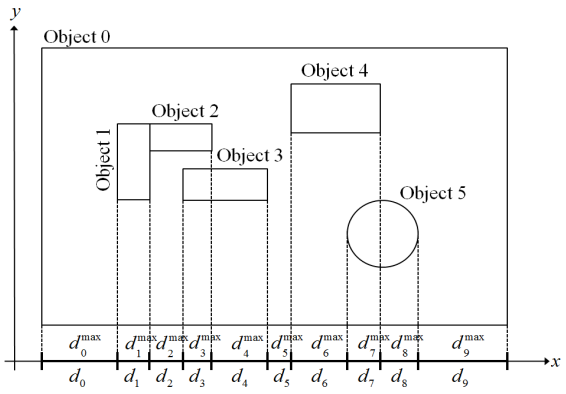

Fig. 1. Projection of objects on the *x*-axis.

† Corresponding Author: School of Electrical and Electronics Eng., Chung-Ang Univ., Korea. (kimcaf2@cau.ac.kr)
* Department of Computer Science and Engineering, Sogang University, Korea. (ihm@sogang.ac.kr)
** Dept. of Electronics Eng., Kangwon National University, Korea. (kyunchoi@kangwon.ac.kr)
Received: October 18, 2010; Accepted: December 8, 2010

3. $\alpha^{\max}$ requirement - The ratios of the lengths of any two adjacent subintervals must be smaller than a user-specified $\alpha^{\max}$ value. This condition is necessary to avoid any possible instability of the analysis process by satisfying the maximum grading ratio constraint.

3. The Proposed Algorithms

3.1 Computation of Feasible Ranges [$e_{i,0}^{\min}$, $e_{i,0}^{\max}$]

Given a set of *m* initial subdivision intervals, tessellation must be applied to these intervals. When considering the *i*th interval, the minimum number of subdivisions is

$$n_i = ceil(d_i / d_i^{\max}) \tag{1}$$

Considering that minimizing the number of 3D cells is a necessary criterion of tessellation, n_i subintervals are initially selected. However, when satisfying the $\alpha^{\max}$ requirement, it is frequently necessary to increase the number of subintervals. For example, two adjacent initial intervals with steeply varying $d_i^{\max}$ values need refinement.

In the presented technique, the interval is tessellated symmetrically, as shown below.

$$e_{i,j} = e_{i,n_i-1-j}, \text{ and } \frac{1}{\alpha^{\max}} \le \frac{e_{i,j}}{e_{i,j+1}} \le \alpha^{\max} \tag{2}$$

where $e_{i,j}$ (j = 0, 1, …, $n_i - 1$) is the length of the *j*th subinterval. Two forms of the tessellation are considered. The first is that the subinterval lengths increase gradually while satisfying the $\alpha^{\max}$ requirement and then, in turn, decrease symmetrically (Case 1). Conversely, in the second case, the subinterval lengths decrease and then increase (Case 2). The key at this stage is to select the length $e_{i,0} = e_{i,n_i-1}$ of the subintervals on the boundaries appropriately.

If the *i*th interval is in the range [$e_{i,0}^{\min}$, $e_{i,0}^{\max}$], which is determined by the $d_i^{\max}$ and the $\alpha^{\max}$ requirements, the lower bound $e_{i,0}^{\min}$ then corresponds to the situation where the maximum $\alpha^{\max}$ value is applied to Case 1. When $\alpha = \alpha^{\max}$,

$$e_{i,0}^{\min} = \begin{cases} 0.5d_i(\alpha-1)/(\alpha^{n_i/2}-1) & n_i \text{ is odd} \\ d_i(\alpha-1)/(\alpha^{(n_i+1)/2}+\alpha^{(n_i-1)/2}-2) & n_i \text{ is even} \end{cases} \tag{3}$$

It is possible that increasing the subinterval length might exceed the upper limit $d_i^{\max}$. If this happens, when n_i is odd, the length of the longest subinterval, which is located at the center, is set to $d_i^{\max}$. The process is repeated using the interval length $d_i - d_i^{\max}$ with $n_i - 1$ intervals. When n_i is even, the process is iterated with interval length $d_i - 2d_i^{\max}$ and $n_i - 2$ intervals, until the length constraints are satisfied.

The upper bound $e_{i,0}^{\max}$ is similarly obtained for Case 2, with $\frac{1}{\alpha^{\max}}$ replacing α in the previous discussion. For the upper bound, the condition $e_{i,0}^{\max} < d_i^{\max}$ must be maintained.

3.2 Algorithm 1

There are now *m* possible ranges [$e_{i,0}^{\min}$, $e_{i,0}^{\max}$], from which each $e_{i,0}$ needs to be selected. One strategy is to assign a properly chosen value $e_{i,0}^*$ identically to all $e_{i,0}$ values with assuming that that the intersection of the *m* ranges is non-empty. Inasmuch as it is desirable to set $e_{i,0}^*$ as large as possible,

$$e_{i,0}^* = \min_{i=0}^{m-1} e_{i,0}^{\max} \tag{4}$$

When the intersection is null, as shown in Fig. 2(a), there exists a range of possible initial subdivision intervals. For example, the first interval, is simply above that of $e_{i,0}^* = e_{2,0}^{\max}$. It is necessary to reduce the interval range by inserting more subintervals, typically, by increasing n_1 gradually, until they intersect with each other. By adapting such undesirable intervals sequentially, $e_{i,0}^*$ can be chosen as desired, with an associated expense of increasing the number of subintervals and, therefore, the number of computations. Once $e_{i,0}^*$ is determined, the proper α_i value is computed for each interval and the tessellation process proceeds.

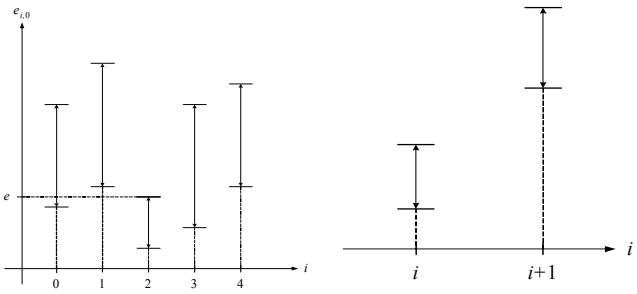

(a) Subinterval Projections (b) Adjacent Subintervals

Fig. 2. Examples of (a) subinterval projections and (b) two adjacent subintervals with a large gap.

3.3 Algorithm 2

Whereas the previous technique easily produces a tessellation which fulfills both the $d_i^{\max}$ and the $\alpha^{\max}$ requirements, the restriction in which all initial subdivision intervals share the same $e_{i,0}$ value is too severe, which often

results in a rapid increasing in the number of subintervals. A more efficient method is to allow each interval to have a distinct $e_{i,0}$ value. We developed a heuristic selection scheme, which reduces the number of generated cells significantly. The main idea is to determine the $e_{i,0}$ values sequentially, starting with the interval where $e_{i,0}^{\max}$ is the minimum.

The selection process consists of two major parts. First, the feasible ranges of initial subdivision intervals are adjusted as necessary, so that the $\alpha^{\max}$ requirement is satisfied between the adjacent intervals. Then, the $e_{i,0}$ values are selected in an appropriate order. Consider two adjacent initial subdivision intervals, i and i+1. If their feasible ranges intersect, the $\alpha^{\max}$ requirement is met, and $e_{i,0}$ and $e_{i+1,0}$ can be chosen properly. Some problem occurs if the ranges are too distant, as shown in Fig. 2(b). It is necessary that $e_{i,0}^{\max} \cdot \alpha^{\max} \geq e_{i+1,0}^{\min}$. If this constraint does not hold, the range needs to be reduced by inserting more subintervals until the inequality is satisfied. This correction process may introduce a similar problem between the next two subintervals, i+1 and i+2.

To solve such a cascade problem, we first select the jth interval with the minimum $e_{j,0}^{\max}$, and scan the other i intervals, reducing them as necessary, so that $e_{j^*,0}^{\max} \cdot \alpha^{|i-j^*|} \geq e_{i,0}^{\min}$. Once this scanning process is finished, the $\alpha^{\max}$ requirement, with respect to the interval j^*, is guaranteed. The process is repeated for all successively larger $e_{j,0}^{\max}$ until the size constraint is satisfied.

It is now possible to determine the $e_{i,0}$ values, starting with the interval having the minimum $e_{i,0}^{\max}$. The other intervals are scanned in the order of increasing $e_{i,0}^{\max}$. Depending on its relation to its neighbors, a proper value is assigned to each $e_{i,0}$ as follows:

1) $e_{i,0}^{\max}$ if both $e_{i-1,0}$ and $e_{i+1,0}$ are not set yet,
2) $\min\{ e_{i-1,0} \cdot \alpha,\ e_{i,0}^{\max} \}$ if $e_{i-1,0}$ is already set, but $e_{i+1,0}$ is not,
3) $\min\{ e_{i,0}^{\max},\ e_{i+1,0} \cdot \alpha \}$ if $e_{i+1,0}$ is already set, but $e_{i-1,0}$ is not, and
4) $\min\{ e_{i-1,0} \cdot \alpha,\ e_{i,0}^{\max},\ e_{i+1,0} \cdot \alpha \}$ if otherwise.

This adaptive assignment produces a more efficient tessellation of the initial intervals.

4. Performance Tests on Mesh Generation

Fig. 3 illustrates three 3D test models that are comprised of cuboids, spheres, and cylinders. As described, each elementary object is projected orthogonally on the three principal axes to determine the initial subdivision intervals and

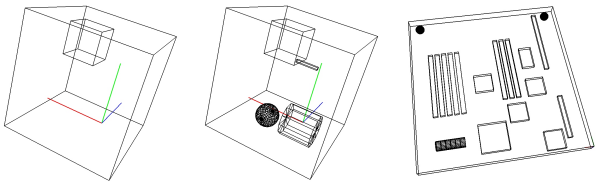

(a) Cuboid (b) Cuboid, Cylinder Sphere (c) Complex

Fig. 3. Three test data sets for performance evaluation.

their $d_i^{\max}$ values. To handle non-regular shapes, such as circles or slanted cuboids, our current implementation uses an axis-aligned bounding box, with its projected intervals inheriting the shape's $d_{\max}$ value. This is a natural choice when the domain is subdivided with axis-aligned elementary cuboids because $d_i^{\max}$ of an interval along an axis needs to be set according to the $d_{\max}$ values of all objects projected on the interval.

The performance characteristics of the mesh generation algorithms are reported in Table 1. The total number of cells in the final FDTD mesh is shown. Additionally, the number of tessellation subintervals on the x-, y-, and z-axes is provided. The grading ratio, $\alpha^{\max}$ = 1.3, was maintained for all geometries. The column labeled "Lower" indicates the optimal lower bound for each quantity, which is determined by the summation of ni and is obtained using Equation 1. This lower bound $\sum_i n_i = \sum_i ceil(d_i / d_i^{\max})$ is often impossible to achieve. Usually, the actual lower bound is higher because of constraints imposed by the d_i and the $d_i^{\max}$ values and by the $\alpha^{\max}$ condition.

Algorithm 1 consists of uniform $e_{i,0}$ values applied to all intervals. In Algorithm 2, the $e_{i,0}$ s were selected adaptively, as described in this paper. As expected, the better

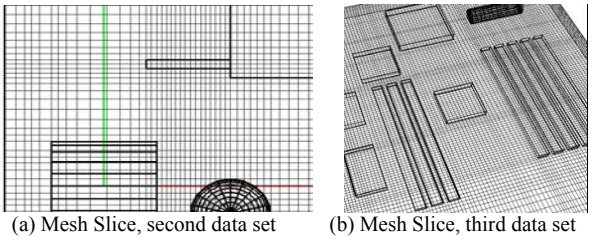

(a) Mesh Slice, second data set (b) Mesh Slice, third data set

Fig. 4. Examples of Projection Planes obtained from Test Data Sets.

Table 1. Performance Statistics

	Test data 1		Test data 2		Test data 3	
	Lower	Alg 1	Lower	Alg 1	Lower	Alg 1
		Alg 2		Alg 2		Alg 2
Cells	23,520	40,392	77,326	370,668	112,320	467,840
		32,736		115,056		131,625
x-axis	28	33	46	68	104	272
		31		51		117
y-axis	28	34	41	69	120	172
		32		48		125
z-axis	30	36	41	79	9	10
		33		47		9

flexibility of Algorithm 2 resulted to significantly better performance. Further, considering the fact that the optimal lower bound cannot usually be realized practically, this mesh generation algorithm is very effective.

5. Numerical Results

To demonstrate the flexibility and the robustness of this mesh generation scheme, an integrated-circuit package antenna (ICPA) is taken for test analysis. Similar structures are presented in [7]-[12]. Such ICPA features miniaturization in physical size while showing good electrical performance in terms of frequency spectrum. An overall configuration of the ICPA is shown in Fig. 5.

The ICPA consists of a supporting substrate with a conductive patch printed on top. It is fed by a coaxial cable of approximately 50Ω. The patch is H-shaped, with two slots located near the horizontal edges. The desired two bands are realized by the first and the third harmonics. The second harmonic should be suppressed by the edge slots. However, because of its high sensitivity to the design parameters, this goal is difficult to achieve in practice, especially when numerical methods are implemented, with the assumed ideal behaviors at corners and edges. The dimensions of the patch are given in Fig. 6.

Based on the information provided in Fig. 5 and 6, we generated 3D mesh distributions using Algorithms 1 and 2. Algorithm 1 is tested to show that it is better than Algorithm 2 on a PC.

The Algorithm 2 took negligible computing time about 0.27 millisecond to generate 278,663 cells with 77, 77, and 47 subintervals in the *x*-, *y*-, and *z*-axes, respectively. Algorithm 1 had 838,488 cells with 138, 124, and 49 subintervals along the axes.

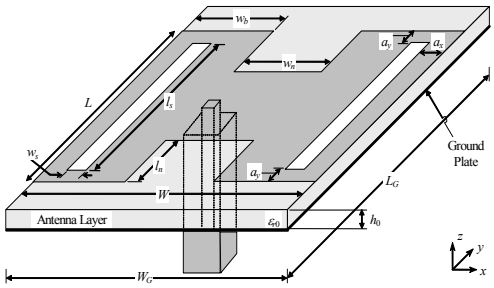

Fig. 5. Configuration of the dual-band ICPA structure.

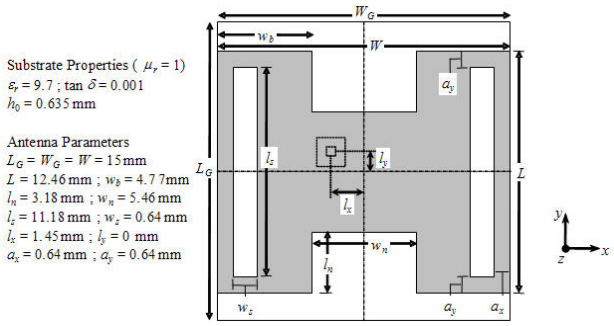

Fig. 6. Configuration of the dual-band ICPA structure (top view).

The magnitudes of the return loss (S_{11}) of Algorithms 1 and 2 are compared with the result of a commercial tool HFSS in Figs. 8(a) and (b). Considering the structure shown in Fig. 5, multi-band resonance dips occur with different sizes of resonating patches. In Fig. 8(a), an excellent agreement is observed. Fig. 8(b) shows that Algorithm 2, with fewer cells, provides the same accuracy as Algorithm 1, which has less cells.

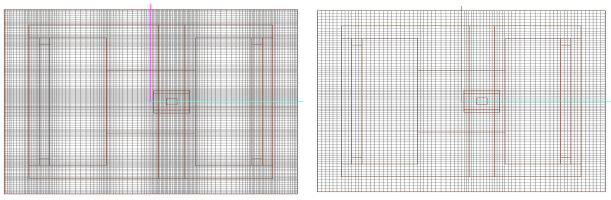

(a) Algorithm 1 (b) Algorithm 2

Fig. 7. Top view of the mesh generated structures of Algorithms 1 and 2.

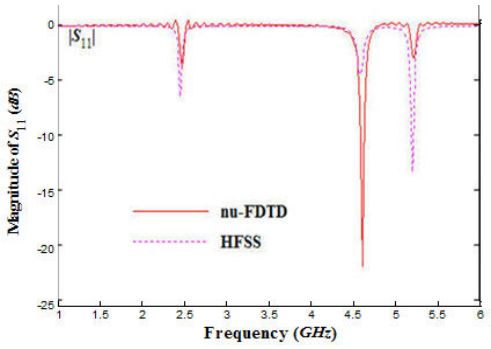

(a) Algorithm 1

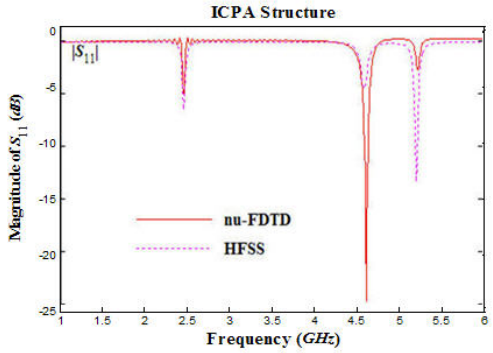

(b) Algorithm 2

Fig. 8. Magnitudes of $|S_{11}|$ for the ICPA structure.

6. Conclusion

A novel method to generate non-uniform finite-difference grids is developed using orthogonal projections which projects initially on the local axial planes with respect to the object geometry and then on the principal axis. The Algorithm 2 which has an adaptive scheme based on

cascading subinterval lengths is proved to be more effective than utilizing uniform subintervals denoted as Algorithm 1 in producing less grid points. The proposed mesh generation techniques have been successfully combined with an in-house FDTD solver to analyze a complicated ICPA. The electromagnetic simulation demonstrated that Algorithm 2 provides better or an equivalent performance compare to the Algorithm 1 with the advantage of a reduced number of cells.

Acknowledgement

We are grateful to Mr. B. Chang for his initial implementation and to Dr. M. S. Tong for his great work on non-uniform FDTD analysis algorithm.

References

[1] A. Taflove and S. C. Hagness, Computational Electrodynamics: The Finite-Difference Time-Domain Method, 2nd ed., Artech House, 2000.

[2] Wenhua Yu, R. Mittra, "Development of a graphical user interface for the conformal finite-difference/ time-domain (CFDTD) software package," *IEEE APM*, Vol. 45, No.1, pp. 58-74, 2003.

[3] M.H. Kermani, O.M. Ramahi, "The complementary derivatives method: a second-order accurate interpolation scheme for non-uniform grid in FDTD simulation," *IEEE MWCL*, Vol. 16, No.2, pp.60-62, 2006

[4] C. Guiffaut, A. Reineix, "Cartesian Shift Thin Wire Formalism in the FDTD Method With Multiwire Junctions," *IEEE Trans. on AP*, Vol. 58, No. 8, pp. 2658-2665, 2010.

[5] Kyung Choi, S.J. Salon, K.A. Connor, L.F. Libelo, S.Y. Hahn, "Time Domain Finite Element Analysis of High Power Microwave Aperture Antenna", *IEEE Trans. on Magnetics,* Vol. 31, No. 3, pp. 1622-1625, 1995.

[6] Kyung Choi, et al., "A Second-Order Accurate Method to a Time Domain Analysis of Wave Propagation in an Irregular Mesh", *IEEE Trans. on Magnetics,* Vol. 32, No.3, pp.938-941, 1996.

[7] Y. P. Zhang, "Integration of microstrip antenna on ceramic ball grid array package," *IEEE EL*, Vol. 38, No. 5, pp. 207-208, 2002.

[8] Y. P. Zhang, "Integration of microstrip antenna on cavity-down ceramic ball grid array package," *IEEE EL*, Vol. 38, No. 22, pp.1307-1308, Oct. 2002.

[9] C. C. Zhang, J. J. Liu, Y. P. Zhang, "ICPA for highly integrated concurrent dual-band wireless receivers," *IEE EL*, Vol. 39, No. 12, pp. 887-889, Jun. 2003.

[10] Y. P. Zhang, "Finite-difference time-domain analysis of integrated circuit ceramic ball grid array package antenna for highly integrated wireless transceivers," *IEEE Trans. on AP*, Vol. AP-52, No. 2, pp. 435-442, Feb. 2004.

[11] Y. P. Zhang, "Integrated circuit ceramic ball grid array package antenna," *IEEE Trans. on AP*, Vol. 52, No. 10, pp. 2538-2544, Oct. 2004.

[12] M. S. Tong, H.-S. Kim, T.-G. Chang, M. Yang, Q. Cao, and Y. Chen, "Design and analysis of integrated-circuit package antenna (ICPA) for concurrent dual-band highly integrated wireless transceivers," *International Journal of RFMICAE*, Vol. 16, No. 3, pp. 250-258, 2006.

Hyeong-Seok Kim was born in Seoul, South Korea, on October 9, 1962. He received his B.S., M.S., and Ph.D. degrees from the Department of the Electrical Engineering of the Seoul National University, Seoul, South Korea, in 1985, 1987, and 1990, respectively. From 1990 to 2002, he was with the Division of Information Technology Engineering, Soonchunhyang University, Asan, South Korea. In 1997, he was a visiting professor at the Electrical Computer Science Engineering, Rensselaer Polytechnic Institute, Troy, New York USA. In 2002, he transferred to the School of Electrical and Electronics Engineering, Chung-Ang University, Seoul, South Korea as a professor. His current research interests include numerical analysis of electromagnetic fields and waves, analysis and optimal design of passive and active components for wireless communication, RFID applications, power information technology, and electromagnetic education.

Insung Ihm is a Computer Science and Engineering professor at Sogang University in Seoul, South Korea. In 1985, he graduated from Seoul National University with a Bachelor's Degree in Computer Science and Statistics. He received his M.S. and Ph.D. degrees in Computer Science from Rutgers University in 1987 and from Purdue University in 1991, respectively. His research interests include computer graphics, scientific visualization, and high-performance computing.

Kyung Choi was born in Taegu, South Korea in 1958. He received his B.S., M.S., and Ph.D. degrees in electrical engineering from Seoul National University, South Korea in 1981, 1983, and 1988, respectively. Since 1989, he has been a professor at Kangwon National University, South Korea, where he is a full professor. He joined Rensselaer Polytechnic Institute (Troy, USA) and University of Washington (Seattle, USA) as a visiting scholar for one year in 1993 and 2008, respectively. His interests include adaptive methods, optimization in numerical methods, and analysis on wave propagations, RF components. He is the corresponding author in this paper.